Modelling of damage in composite materials using interface elements

Authors:

W.G. Jiang, Department of Aerospace Engineering, University of Bristol
S.R. Hallett, Department of Aerospace Engineering, University of Bristol
M.R. Wisnom, Department of Aerospace Engineering, University of Bristol

Correspondence:

W.G. Jiang, Department of Aerospace Engineering, University of Bristol,
Queens Building, University Walk, Bristol, BS8 1TR
Tel: 0117 9287696
Fax: 0117 9272771
w.jiang@bristol.ac.uk

Keywords:
delamination, progressive failure analysis, interface elements

ABSTRACT

A simple and robust implementation of an interface element has been addressed in this paper. A new state variable is introduced to trace the extent of damage accumulated at the interface. The element not only simulate mixed mode delamination propagation in composite materials but also satisfactorily deals with mode ratio change during the debonding process. The interface model is implemented in LS-DYNA code. The model has been applied to scaled open hole tension tests. Comparison between numerical results and experiments shows good correlation.

INTRODUCTION

The effect decreasing strength with increasing specimen size in composite materials is a well documented phenomenon [1]. With the increasing use of large composite components in aerospace applications comes the need for reliable design methods to be able to extrapolate data from small scale laboratory tests to full size components, thus reducing the need for full-scale testing. Holes are required in aircraft components for joints, access, or to allow the passage of wires and hydraulics. An extensive testing program has been conducted at the University of Bristol to investigate the influence of specimen size on the open hole tensile strength of composites and the mechanisms behind variations [2]. It has been found that delamination and splitting play a significant role in determining the strength of a laminate.

The traditional virtual crack closure technique (VCCT) [3] based on linear elastic fracture mechanics has been successfully used in the prediction of delamination growth [4]. However the use of this technique requires that an initial delaminated area must be predefined and only self-similar delamination growth can be dealt with satisfactorily. To overcome the limitation associated with VCCT, an interface element has been developed in LS-DYNA. The interface elements are located between adjacent laminae of a laminated composite structure to simulate both initiation of delamination and non-self-similar growth of delamination cracks without specifying an initial delamination. A bilinear softening cohesive-decohesive constitutive law which relates the interfacial traction components to the displacement components has been implemented.

The failure of the interface element under mixed mode condition is defined by a power law using experimentally determined fracture energies without the need for further curve fitting parameters. A simple new state variable is introduced to trace the damage accumulated at the interface. Since composite delamination processes often involve strong nonlinear events such as snap-back and snap through, convergence is usually very difficult to achieve if the simulations are performed using an implicit code without complex path following algorithms [5]. The use of an explicit solver such as LS-DYNA overcomes many of these difficulties.

This paper describes the formulation of the interface element, its application in models of the experimental programme and results obtained which show good correlation to location, extent and failure stress of delamination and splitting which occurs.

CONSTITUTIVE EQUATIONS

The stress singularities predicted by FE at a crack tip in the linear elasticity solution cannot be reconciled with any realistic local rupture process. The softening type of cohesive zone model presented here is intended to represent the degradation of the material ahead of the crack tip. It captures strength-based bond weakening, and fracture-based bond rupture.

The softening constitutive law is implemented within an interfacial surface material consisting of a pair of bonded surfaces S^+ and S^- connected by continuous distributed nonlinear springs (see Figure 1). The bilinear interface formulation adopted in this paper for mixed-mode softening law can be illustrated in a single three-dimensional map by representing open mode (Mode I) on the 0 - σ - δ_{normal} plane, and shear mode (mode II) on the 0 - σ - δ_{shear} plane, as shown in Figure 2. The triangles 0 - T - $\delta_I^{\max}$ and 0 – S - $\delta_{II}^{\max}$ are the bi-linear response in pure open mode and in pure shear mode respectively. Any point on the 0 - δ_{normal} - δ_{shear} plane represents a mixed-mode relative displacement.

The total mixed-mode relative displacement is defined as:

$$\delta_m = \sqrt{\delta_I{}^2 + \delta_{II}^2} \tag{1}$$

where $\delta_I = \max(\delta_1, 0)$ is the normal opening relative displacement, $\delta_{II} = \sqrt{\delta_2^2 + \delta_3^2}$ the resultant shear relative displacement. δ_1, δ_2 and δ_3 are relative displacement components for a pair of interface connecting points in a local orthogonal coordinate system. δ_1 is the component normal to interface mid-plane (see Figure 1).
The damage initiation under a multi-axial stress state adopted is:

$$\left(\frac{\max(\sigma_I, 0)}{\sigma_I^{\max}}\right)^2 + \left(\frac{\sigma_{II}}{\sigma_{II}^{\max}}\right)^2 = 1 \tag{2}$$

where σ_I is the normal interlaminar tensile stress, σ_{II} the shear stress resultant of the interface, $\sigma_I^{\max}$ the interlaminar tensile strength, and $\sigma_{II}^{\max}$ the interlaminar shear strength. We assume that the normal interlaminar compressive stress does not affect to the onset of delamination. The damage initiation locus represented by the relative displacement corresponding to softening onset, δ_m^e, can be determined by this condition (see figure 2).

The failure criterion of interface element under mixed mode condition used is defined by the power law proposed by Whitcomb [6]:

$$\left(\frac{G_I}{G_{IC}}\right)^{\alpha} + \left(\frac{G_{II}}{G_{IIc}}\right)^{\alpha} = 1 \tag{3}$$

where $\alpha \in (1.0 \sim 2.0)$ is an empirical parameter derived from mixed-mode tests, G_{IC} and G_{IIC} are critical energy release rates for mode I (open) and mode II (shear) respectively. The fully debonded locus represented by the relative displacement corresponding to the complete interface failure, $\delta_m^{\max}$, can be determined by this condition (see figure 2).

A simple new state (or history) variable *d* is introduced to track the extent of damage accumulated at the interface:

$$d(\delta_m) = \frac{\delta_m - \delta_m^e}{\delta_m^{\max} - \delta_m^e} \tag{4}$$

Its initial value is ${}^0d = 0$ and will remain zero until the damage initiation condition (2) is met. It is a monotonically increasing value which starts to grow when $\delta_m > \delta_m^e$ and reaches the failure value 1 when $\delta_m \geq \delta_m^{\max}$.

The state variable *d* is defined in such a way as to assure that transition between load steps is smooth, even for the case of significant mode ratio change. To complete the constitutive law, unloading is simply assumed to return linearly back to zero stress state at the origin as shown in Figure 2.

FINITE ELEMENT ANALYSES AND COMPARISON WITH TESTS

It is well known that the strength of composites is related to the size of the specimen tested. To study the size effects, a series of scaled specimens manufactured from Carbon-Fibre epoxy were tested and analyzed. A symmetric quasi-isotropic lay-up with ply orientations of $(45°/90°/-45°/0°)_s$ was used. Laminate thickness was increased by increasing the thickness of each of the individual ply blocks. The geometry and dimensions are given in Figure 3. The rectangular laminates with a centrally located circular hole subjected to tension were modelled with eight noded fully integrated brick elements using LS-DYNA software. To reduce the model size, only the gage length was modelled. Since the layup is symmetric, it was only necessary to model half the thickness. Plane symmetric boundary condition on the mid-plane of the laminates were applied.

Duplicate nodes are placed on either side of any adjacent ply interfaces where delamination is expected, and these are connected together with interface elements to model delamination between plies [7]. A similar method is used to model splitting which occurs between fibres within a ply by means of interface elements which are located in the sites where the splits were found to occur from the tested samples [2], see Figures 4 and 5. The properties used for the interface elements were taken to be G_{IC}=0.2N/mm, G_{IIC}=1.0N/mm, α=1.0, $\sigma_I^{\max}$=60MPa, $\sigma_{II}^{\max}$=90MPa.

The material properties of individual layers of IM7/8552 carbon/epoxy on the principal material coordinates are taken to be E1=161GPa, E2=E3=11.38GPa, G12=G13=5.17GPa, G23=3.98GPa, ν12=ν13=0.32, ν23=0.436 [8]. The thermal expansion coefficients are α11=0.0, α22=α33=3x10^{-5} °C^{-1}. To include the thermal residual stress from the fabrication of the laminate in the analysis, thermal load (temperature drop, -160°C) was applied first prior to mechanical extension.

A relatively fine mesh was used adjacent to the central hole of the sample, with larger elements away from the notch to reduce the model size. Figure 6 shows a reduced density in-plane mesh. The coarse in-plane mesh shown is denoted as “mesh density 1x1”. Finer meshes are denoted as “mesh 2x2”, and “mesh 3x3” respectively. A mesh sensitivity analysis through the thickness showed that using one element per ply in the through thickness direction is adequate (Figure 7).

Figure 7 shows typical load-extension curves predicted using three different mesh densities for the specimen with hole diameter d=3.175 mm and laminate thickness t=4 mm. The delamination and splitting process for this specimen is also illustrated in Figure 8. All the featured loading stages (marked A to G in

Figure 7) are included. The two 45° splits which are tangent to the hole boundary within the 45° surface ply occured at very low load level (stage A). At stage C, the delamination between 45°/90° started to develop from the splits, and the 90°, -45° and 0° splits within their corresponding plies were all formed close to the hole boundary. At stage D, the -45° and 90° splits had formed completely across the specimen width, the triangular areas within the 45°,/90° and 90°/-45° interfaces were delaminated, and the -45°/0° interface was partially delaminated in one side of the specimen. The split crack front in the 0° ply is acompaning the -45°/0° delamination. The non-symmetric delamination phenomenon between the -45° and 0° plies was also observed in the tests. The peak load before significant delamination damage prediction (loading point C) for all specimens showed good correlation with the test failure load (first load peak before 5% load drop), with exception for the small thin sample (d=3.175mm, t=1mm), see Figure 9. Further investigation shows that the failure mechanism for this sample is due to fibre failure before delamination, which has not yet included in the current finite element model.

SUMMARY AND CONCLUSIONS

An interface element with a bi-linear softening law for mixed mode delamination was proposed and implemented in LS-DYNA. The constitutive equation proposed uses a new single damage variable to track the extent of damage at the interface under general loading conditions. This model has been applied to a series of scaled samples. The finite element model proposed can capture the important features of the progressive delamination processes involved and good agreement has been obtained for delamination strength predictions.

ACKNOWLEDGEMENTS

This work was supported by the UK Engineering and Physical Sciences Research Council, Ministry of Defence and Airbus UK.

REFERENCES

1. Wisnom M.R., Size effects in the testing of fibre-composite materials, Composite Sciences and Technology, Vol. 59, N0. 13, 1937-1957, 1999.
2. Green B., Wisnom M.R., Hallett S.R., Tensile scaling effects in notched composites, 2nd International conference on composites testing and model identification, Paper No. 19, 21-23 September 2004, University of Bristol, UK.
3. Rybricki E.F., Kanninen, M.F., A finite element calculation of stress intensity factors by a modified crack closure integral, Engineering Fracture Mechanics, Vol. 9, 931-938, 1977.
4. Krueger R., O'brien T.K., A shell/3D modeling technique for the analysis of delaminated composite laminates, Composites: Part A, Vol. 32, 25-44, 2001.
5. Alfano G., Crisfield M.A., Finite element interface models for the delamination analysis of laminated composites: mechanics and computational issues, International Journal for Numerical Methods in Engineering, Vol. 50(7), 1701-1736, 2001.
6. Whitcomb J.D., Analysis of instability-related growth of a through-width delamination, NASA TM 86301, 1984.
7. Wisnom M.R., Chang F.K., Modelling of splitting and delamination in notched cross-ply laminates. Composites Science and Technology, Vol. 60, 2849-2856, 2000.
8. O'brien T.K., Krueger R., Analysis of ninety degree flexure tests for characterization of composite transverse tensile strength, NASA.TM-2001-211227 ARL-TR-2568, October 2001.

Figure 1. Schematic of interface element

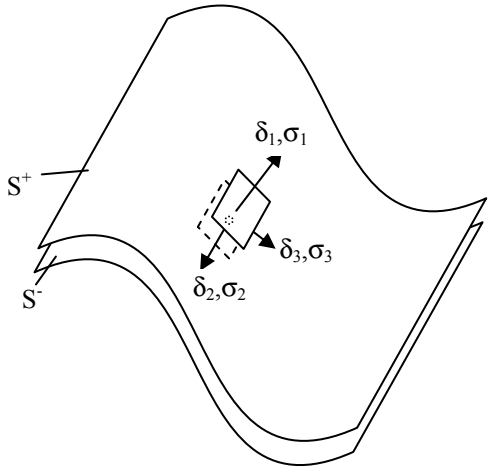

Figure 2. Interfacial bilinear mixed mode softening law

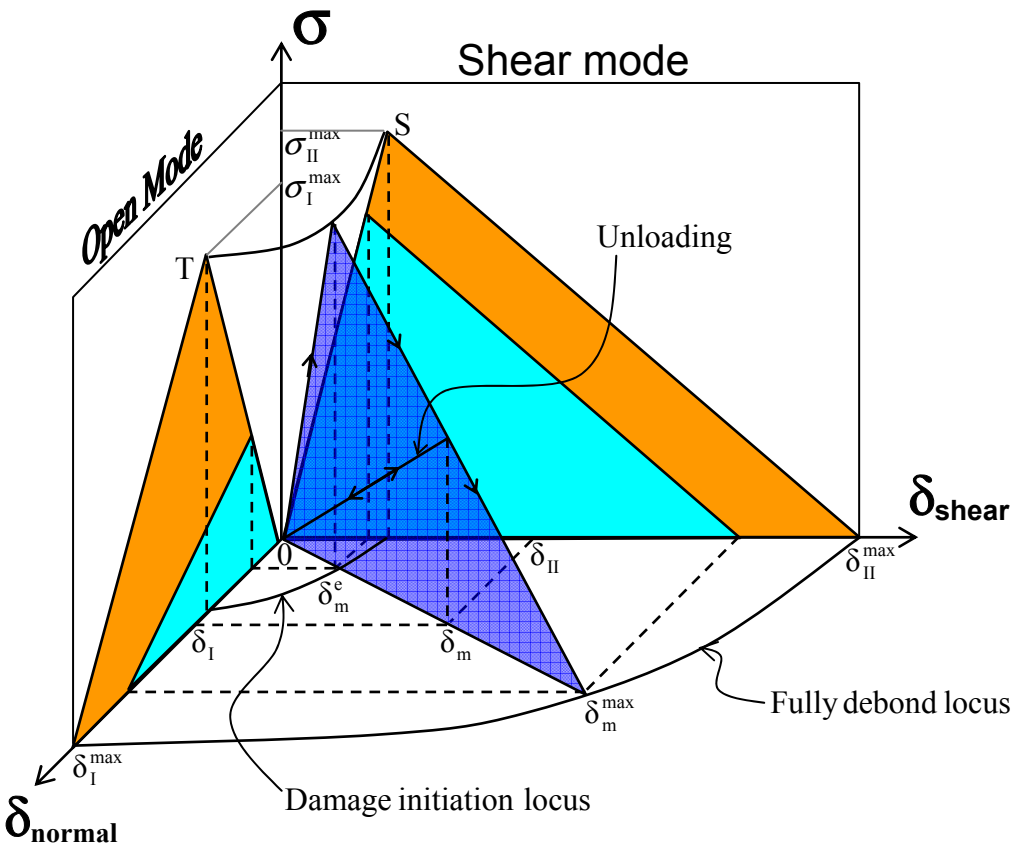

Figure 3. Test specimen geometry [2]

Laminate thickness, t (mm)	Hole diameter, d (mm)		
	3.175	6.35	12.7
1	√		
2	√	√	
4	√	√	√
√ = Configuration tested			

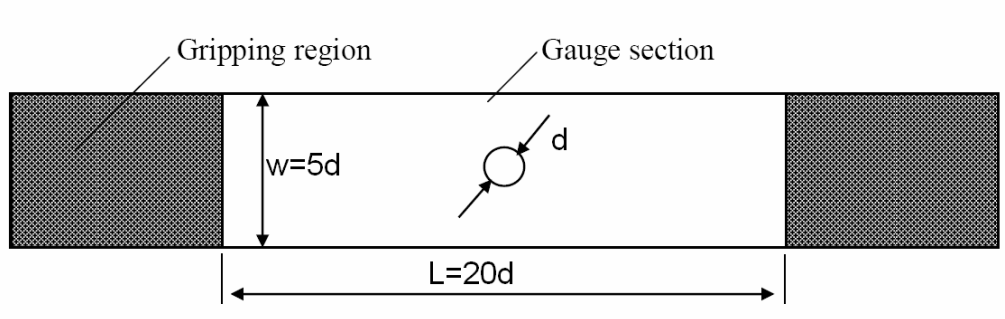

Figure 4. Simplified geometry of the sample modelled

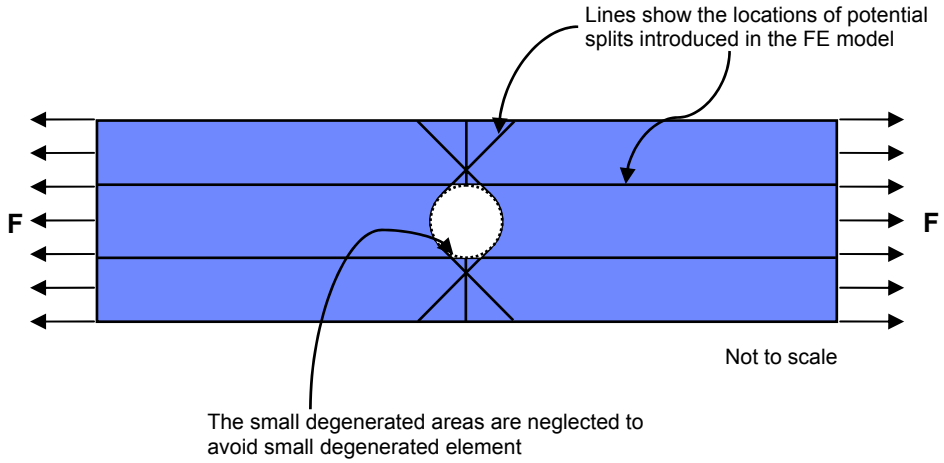

Figure 5. A tested sample showing typical failure mode [2]

Figure 6. Sample finite element mesh (in-plane mesh, mesh density 1x1)

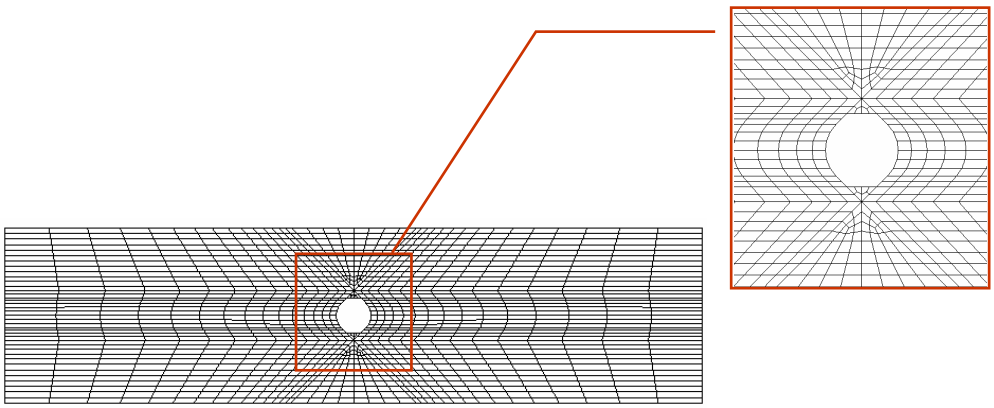

Figure 7. Sample load-extension curve showing the mesh convergence

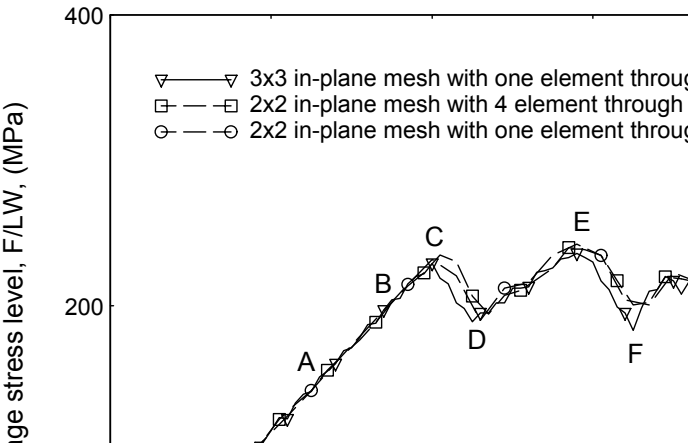

Figure 8. Typical delamination and splitting developing progress from FEM

Loading stage in Fig. 7 (Extension strain %)	Stress level (MPa)	Location of interlaminar interface			Location of splitting within plies
		45°/90°	90°/-45°	-45°/0°	All layers (superimposed)
A (0.25)	141				
B (0.35)	204				
C (0.40)	229				
D (0.45)	189				
E (0.60)	230				
F (0.65)	183				
G (0.84)	262				

Figure 9. Comparison of failure stress level